Redistributed Allocation for Flight Control Failure on a Coaxial Helicopter

Michael McKay PhD Candidate
Praneet Vayalali PhD Candidate
Farhan Gandhi Redfern Professor, Director
Center for Mobility with Vertical Lift (MOVE)
Rensselaer Polytechnic Institute, Troy, NY
Tom Berger Flight Controls Group Lead
Mark J. S. Lopez Aerospace Engineer
U.S. Army Combat Capabilities Development Command
Aviation & Missile Center
Moffett Field, CA

ABSTRACT

An elastic blade flight dynamics model for a coaxial helicopter based on the Sikorsky X2 Technology™ Demonstrator is presented and validated with steady trim and frequency response flight test data. A full authority explicit model following control architecture along with weighted pseudoinverse control allocation is implemented for the model in hover and cruise at 180 knots using CONDUIT® in order to stabilize the vehicle and meet a set of stability, handling qualities, and performance requirements. Different fault scenarios are considered including failure of rotor swashplate actuators and tail surface actuators in hover and forward flight, which are compensated for by recalculating the pseudoinverse control mixing accordingly. The approach is shown to maintain aircraft stability through the fault transient and into a new steady trim state for the vehicle. Though the implemented controller is successful in maintaining the aircraft state, different fault cases lead to violations in rotor tip clearance limits, which will require additional effort to account for in flight.

NOTATION

n_z	Stability Axis Vertical Acceleration (g)
s_{aft}	Aft Swashplate Actuator Position (%)
s_{lat}	Lateral Swashplate Actuator Position (%)
s_{fwd}	Forward Swashplate Actuator Position (%)
T_{prop}	Propeller Thrust (lb)
δ_{lat}	Lateral Mixer Input
δ_{lon}	Longitudinal Mixer Input
p	Body Frame Roll Rate (deg/s)
q	Body Frame Pitch Rate (deg/s)
Γ	Swashplate Control Phase Angle (deg)
δ_e	Elevator Deflection (deg), positive TE down
δ_r	Rudder Deflection (deg), positive TE left
θ_0	Symmetric Collective Pitch (deg)
θ_{Lon}	Symmetric Longitudinal Pitch (deg)
θ_{Lat}	Symmetric Lateral Pitch (deg)
$\Delta\theta_0$	Differential Collective Pitch (deg)
$\Delta\theta_{Lon}$	Differential Longitudinal Pitch (deg)
$\Delta\theta_{Lat}$	Differential Lateral Pitch (deg)

Presented at the Vertical Flight Society's 77th Annual Forum & Technology Display, Virtual, May 10–14, 2021.

INTRODUCTION

High speed coaxial helicopters are poised to revolutionize the future of vertical flight. The ability of this aircraft type to perform typical VTOL missions as well as push the flight envelope and mission capabilities into a high-speed regime is a feat rotary wing vehicles have traditionally been unable to perform. With the establishment of the Department of Defense Future Vertical Lift (FVL) initiative (Ref. 1), coaxial-pusher helicopters have become an area of recent interest. This non-traditional VTOL aircraft has the ability to fly farther, faster, and longer than the current fleet of rotorcraft being utilized. Under the Joint Multi-Role Technology Demonstrator program, these vehicles are being built and tested in order to study and improve these future concepts.

A unique feature of these aircraft, as well as other advanced rotorcraft concepts, is the availability of multiple redundant effectors typically not present on legacy rotary wing vehicles. These enable the aircraft to achieve non-unique trim states that can be varied depending on the objective of the mission or in order to compensate for a component failure in the other flight controls. In recent work, the ability to utilize redundant controls for power minimization, load alleviation, and noise reduction has been explored on different FVL type platforms. Different studies performed at RPI have considered power and vibration reduction using redundant controls on the XH-59A coaxial helicopter (Ref. 2) and a compounded UH-60 Black Hawk (Refs. 3, 4). Additional work has been performed at the University of Maryland for optimal multi-objective trim

on the generic coaxial platform (Refs. 5, 6), considering performance, loads, and noise.

Outside of trim simulations, there has also been substantial effort made to develop flight simulation models of coaxial-pusher aircraft for flight control design and handling qualities evaluation. These studies range from development of generic models (Ref. 7) to development and improvement of specific models of the X2 Technology™ Demonstrator in a collaborative effort between the US Army and Sikorsky (Refs. 8, 9). In addition to the modeling effort, significant work has gone into inner and outer loop flight control design for high-speed vehicles, including coaxial helicopters (Refs. 10, 11) outside of the internal development undertaken during production and flight testing of the FVL candidates. These studies highlight the specific challenges (stability, tip clearance, response types) present in the control design of coaxial helicopter platforms and provide potential approaches to achieve good handling qualities performance.

Recently, work at RPI has investigated the use of redundant controls for fault compensation after an actuator lock in the swashplate of a compound helicopter in trim (Ref. 12) and in dynamic simulation (Ref. 13). Previously, the same group demonstrated the ability to compensate for flight control failure on the UH-60A (Refs. 14, 15), demonstrating that the extra controls present can allow for recovery and steady level flight after a component failure in certain flight conditions. In addition to this body of work, the US Army and Piasecki have published a study considering damage tolerant control on the Piasecki X-49A (Ref. 16), where multiple control allocation techniques were implemented and compared for different fault scenarios in piloted simulation.

There is no substantial body of work investigating the use of redundant control effectors to compensate for component failure in different flight conditions for a lift-offset coaxial-pusher helicopter. The present study seeks to build off of prior publication by the authors (Ref. 17), where the ability of a coaxial helicopter to trim post control failure was investigated, and examine the potential use of redundant control allocation to compensate for failure in the available flight controls, considering the method of control allocation and potential fault cases where a redefinition of the allocation can allow for safe recovery of the vehicle.

FLIGHT DYNAMICS MODEL

Simulation results are obtained from the RPI Coaxial Helicopter Analysis and Dynamics (CHAD). The code utilizes a blade element theory model coupled with a pressure potential superposition inflow model (PPSIM, Ref. 18) to calculate rotor forces and moments for a given operating condition and control input. This rotor model has been presented and validated in prior publication by the authors (Ref. 17) against coaxial rotor test data from NACA (Ref. 19) and UT Austin (Ref. 20). The aircraft fuselage and control surfaces are modeled according to the published XV-15 simulation model (Ref. 21), with appropriate scaling to represent the vehicle being considered, which is the X2 Technology™ Demonstrator (X2TD) in the present study. Assumed geometry is provided in Table 1. Finally, the pusher propeller is modeled with momentum theory with appropriate consideration for non-ideal losses in order to match published flight test data. Overall, the CHAD bare-airframe model has a total of 50 states: 12 rigid body, 32 rotor (2 blade modes $\times$ 4 blades $\times$ 2 rotors $\times$ 2), and 6 main rotor inflow (3 states per rotor). Model validation is presented in a following subsection.

Table 1. Coaxial Model Details

Aircraft	
Gross Weight	5,300 lb
Horizontal Tail Area	30 ft^2
Vertical Tail Area	17 ft^2
Rotor	
Radius	13.2 ft
N_b/Rotor	4
Hub Separation	14% R
Ω (Hover)	448 RPM
M_{tip} Limit	0.9
Pusher Prop	
Radius	3.3 ft (0.5 m)
N_b	6
σ	0.2
Ω	2,000 RPM

Rotor Controls and Swashplate Representation

The rotor controls as defined in this study represent the inputs to the rotor head and contain a constant 37.5° control phase angle (Γ) that is typically seen to absorb the phase lag associated with rotor blade dynamics and aerodynamic interference effects. For a typical rotor, there are 3 independent controls traditionally represented by a collective pitch as well as two cyclic inputs. In most helicopter control systems, these controls define the blade pitch at any point about the azimuth as

$$\theta(\psi) = \theta_0 + \theta_{1c}\cos(\psi+\Gamma) + \theta_{1s}\sin(\psi+\Gamma), \qquad (1)$$

where θ_0 is the collective and θ_{1c} and θ_{1s} are the one per revolution cosine and sine cyclic pitch inputs to the rotor. When a dual rotor system is considered, there now exist 6 independent controls to the rotor system, which can be represented as the 3 unique controls for each of the two rotor heads or some combination of controls as desired in the design of the flight controls.

For the purposes of this study, the coaxial rotor controls will be defined as follows in Table 2.

With these controls, the individual rotor pitch variation can be described as in Eqs. 2 and 3.

$$\begin{aligned}\theta_U(\psi_U) = (\theta_0+\Delta\theta_0)+(\theta_{lon}+\Delta\theta_{lon})\cos(\psi_U+\Gamma)\\ +(\theta_{lat}+\Delta\theta_{lat})\sin(\psi_U+\Gamma),\end{aligned} \qquad (2)$$

$$\begin{aligned}\theta_L(\psi_L) = (\theta_0-\Delta\theta_0)+(\theta_{lon}-\Delta\theta_{lon})\cos(\psi_L+\Gamma)\\ -(\theta_{lat}-\Delta\theta_{lat})\sin(\psi_L+\Gamma).\end{aligned} \qquad (3)$$

Table 2. Coaxial Rotor Controls

Control	Description
θ_0	Symmetric Collective
θ_{lon}	Symmetric Longitudinal
θ_{lat}	Symmetric Lateral
$\Delta\theta_0$	Differential Collective
$\Delta\theta_{lon}$	Differential Longitudinal
$\Delta\theta_{lat}$	Differential Lateral

Note that the rotor head control naming convention is opposite to standard convention, where the lateral and longitudinal cyclic inputs are named from the predominant flap response, and so are the cosine and sine component of the cyclic input, respectively. Here, due to the large stiffness of the rotor and choice of control phase angle, the cosine and sine components of the cyclic input result in dominant *on-axis* flap responses, and so are named longitudinal and lateral for the present study.

Another key component in the rotor controls is the swashplate actuator geometry. To this end, a generic swashplate geometry is developed to analyze different flight conditions and potential limiting situations for the rotor system. The derivation is simple, requiring the minimum and maximum collective pitch allowable at the rotor head as well as the azimuthal positions of the swashplate servo actuators on the non-rotating swashplate.

First, consider the normalized throw of a servo actuator, that is $s \in [0,1]$. Note that if all actuators are in the minimum position, the blade pitch will by definition exist at the minimum allowable collective setting, it follows similarly for the maximum servo position and maximum collective setting. Defining this allowable collective range as $\theta_0 \in [\theta_{min}, \theta_{max}]$, it follows that at the azimuthal position of the i^{th} servo, the blade root pitch is

$$\theta(\psi_i) = (\theta_{max} - \theta_{min})s + \theta_{min}. \tag{4}$$

Equating the above expression and Eq. 1 for the local blade root pitch gives the mapping from actuator to rotor head controls as

$$T_{\theta/s}\begin{bmatrix} s_1 \\ s_2 \\ s_3 \end{bmatrix} + b_{\theta/s} = T_\theta \begin{bmatrix} \theta_0 \\ \theta_{1c} \\ \theta_{1s} \end{bmatrix}, \tag{5}$$

$$T_{\theta/s} = (\theta_{max} - \theta_{min}) \begin{bmatrix} 1 & 0 & 0 \\ 0 & 1 & 0 \\ 0 & 0 & 1 \end{bmatrix}, \tag{6}$$

$$b_{\theta/s} = \begin{bmatrix} \theta_{min} & \theta_{min} & \theta_{min} \end{bmatrix}^T, \tag{7}$$

$$T_\theta = \begin{bmatrix} 1 & \cos(\psi_1+\Gamma) & \sin(\psi_1+\Gamma) \\ 1 & \cos(\psi_2+\Gamma) & \sin(\psi_2+\Gamma) \\ 1 & \cos(\psi_3+\Gamma) & \sin(\psi_3+\Gamma) \end{bmatrix}. \tag{8}$$

Note that this is a generalized and simple representation of a swashplate, in reality swashplate geometry is more complex with other limitations defining the relation between actuator position and rotor head controls. This relation, however, allows for extraction of the general relation between actuators (in certain positions) and rotor head controls, which can assist in identifying flight conditions where actuators may be at relatively extreme positions. The ability to translate pitch control to actuator position can also allow for the identification of ranges of positions that exist throughout large portions of the flight envelope, which can imply aircraft trim for a locked swashplate actuator.

For the present study, the swashplate actuators are assumed to be located at -Γ (322.5°), 90°-Γ (52.5°), and 180°-Γ (142.5°) in the appropriate swashplate azimuthal coordinate. These actuators are consequently labeled s_{aft}, s_{lat}, and s_{fwd} for each rotor, corresponding to the location of the flap response produced by the actuator. The results that follow assume an allowable collective setting range from -5 to 15 degrees on each rotor, which results in a $\pm 10°$ range in θ_{1c} and $\pm 20°$ in θ_{1s} according to the defined model.

Trim Validation

Trim predictions match flight test data quite well and perform similar to other comprehensive codes (Sikorsky GenHel and HeliUM). Predicted rotor and propeller power are compared in Fig. 1, with rotor lift offset and tip clearance plotted in Figs. 2 and 3. Small differences exist in the rotor and propeller power consumption in the low to mid speed range (50-100 knots), which is likely due to the lack of rotor-fuselage and rotor-tail aerodynamic interference resulting in a slight misprediction of rotor and body loads in this speed range. Additionally, the lift offset of the vehicle does not pass directly through flight test data in a similar range, though it should be noted that the lift offset prediction from CHAD is a result of the scheduled trim target, and for all speeds where the target passes through the flight test data, the tip clearance also matches quite well.

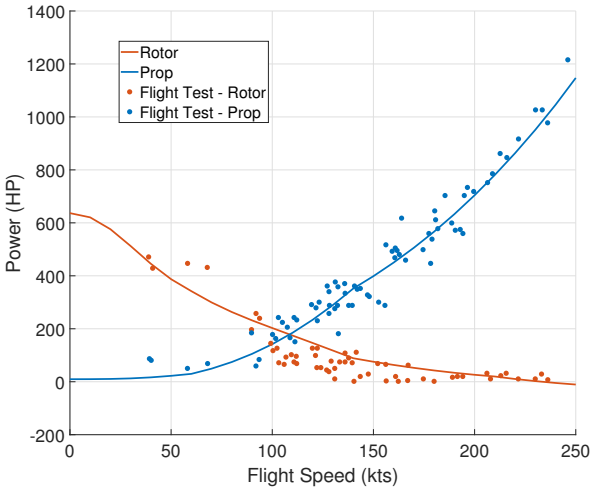

Figure 1. Trim Power Comparison (Ref. 22)

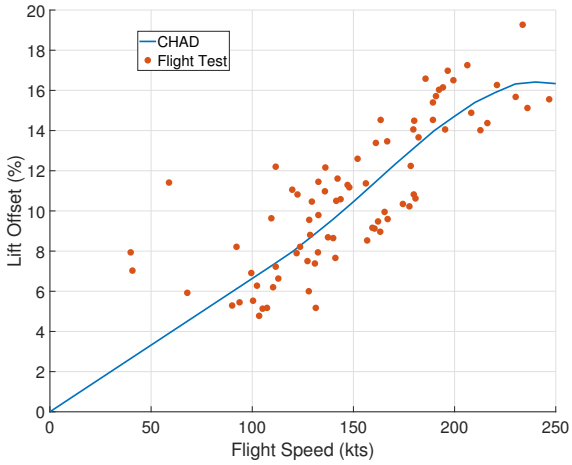

Figure 2. Trim Lift Offset Comparison (Ref. 22)

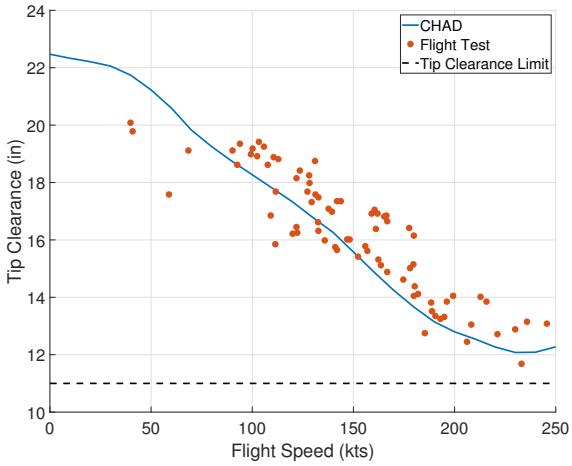

Figure 3. Trim Tip Clearance Comparison (Ref. 22)

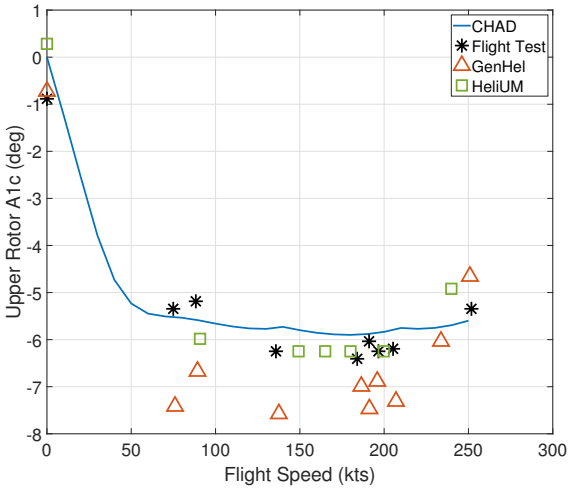

Figure 4. Upper Rotor A1C Comparison (Ref. 8)

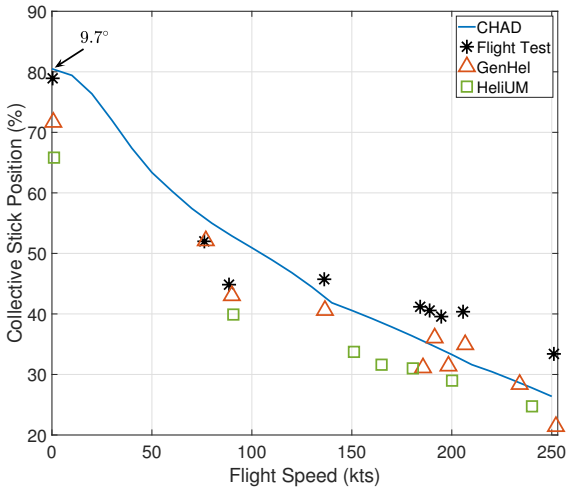

Figure 5. Collective Stick Comparison (Ref. 8)

There are slight differences in the predicted A1C = $-\theta_{1c}$ (Fig. 4) for the rotor relative to flight test as well as in the collective setting (Fig. 5), but these can be attributed to the estimation of certain parameters for the implemented model, the capabilities of PPSIM, as well as the lack of aerodynamic interference between the different vehicle components (rotor-fuselage-tail).

Frequency Response Validation

Open loop frequency responses are compared in the lateral and longitudinal axes against flight test data both in hover and in cruise (180/200 kts). Overall, the frequency behavior is well predicted, with a few notable differences. Note that frequency responses depicted here other than those extracted from CHAD are provided in Ref. 8, along with relevant coherence data. First, there is additional gain and phase roll-off at high frequency in hover for both roll and pitch rate response to stick input relative to flight test and the other comprehensive codes presented (Figs. 6 and 7). This is primarily attributed to the use of averaging in the rotor loads to obtain the vehicle accelerations. However, the hovering cubic peak frequency and the location of the dominant blade modes are well predicted, which are both important for control system design. The estimated hovering cubic peaks are observed at 0.21 Hz for the flight test data and predicted at 0.24 Hz from CHAD. Additionally, the magnitude dip at higher frequency associated with the lead-lag dipole is at 2.3 and 1.8 Hz for roll and pitch rate flight test response, versus 2.8 Hz for both axes from CHAD (Figs. 6 & 7).

In cruise (Figs. 8 and 9), the overall character of the frequency response is well predicted, with a notable difference in the damping ratio of the dutch roll mode (peak magnitude at 0.9 Hz) in the lateral axis. This difference is primarily attributed to uncertainty in the empennage sizing for the model. The general agreement with the flight test data gives confidence to subsequent simulation results.

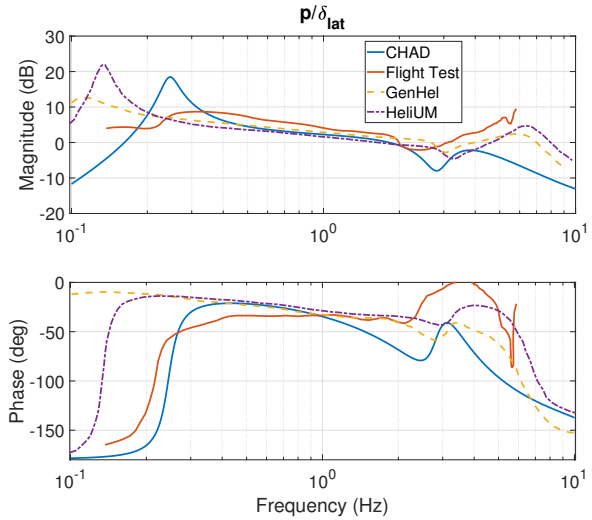

Figure 6. Roll Rate Response to Lateral Stick, Hover (Ref. 8)

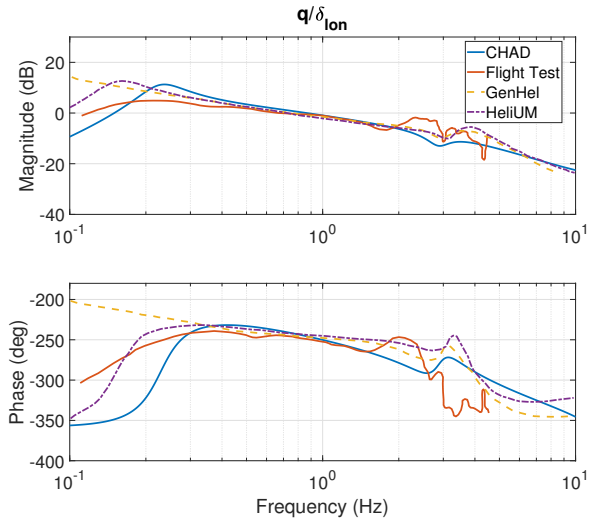

Figure 7. Pitch Rate Response to Longitudinal Stick, Hover (Ref. 8)

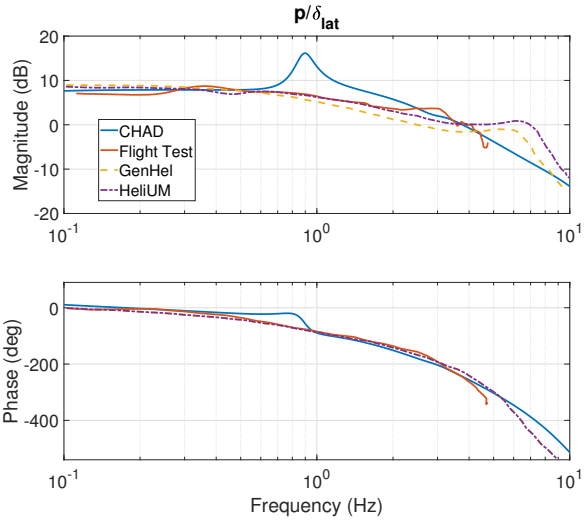

Figure 8. Roll Rate Response to Lateral Stick, 180 kts (Ref. 8)

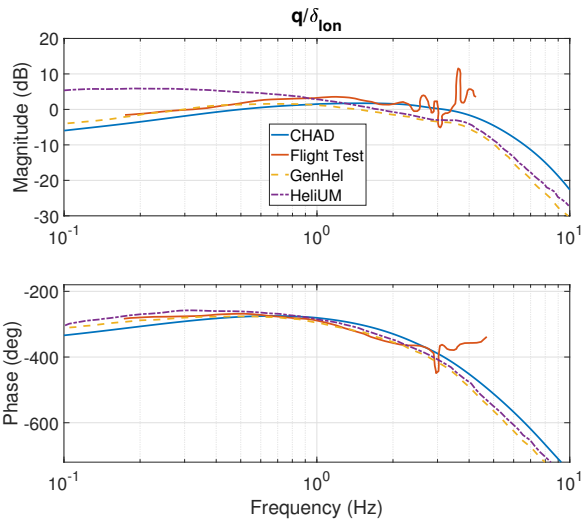

Figure 9. Pitch Rate Response to Longitudinal Stick, 200 kts (Ref. 8)

CONTROL ARCHITECTURE

Linearized aircraft models are extracted from CHAD in hover and cruise and are stabilized and controlled with an explicit model following (EMF) control architecture. This design is chosen for its wide use in modern aircraft control problems as well as the ease of independently tuning performance and disturbance rejection characteristics. A basic overview of the control system is given in Fig. 10. Two flight conditions are considered, hover and 180 kts, and different response types are designed for each case, outlined in Table 3. The control system is designed similar to the architecture designed for the US Army generic coaxial model, presented in Ref. 10.

The design parameters of the control system are optimized with the Control Designer's Unified Interface, CONDUIT® (Ref. 23). This software optimizes the feedback gains in the system to meet a set of stability, handling-qualities, and performance specifications, listed in Table 4. Note that in cruise, the stability margin requirement in pitch had to be relaxed due to the bare airframe dynamics at this condition, this was also done for the US Army generic coaxial model in Ref. 10 above 260 knots.

Control Allocation

The coaxial helicopter has control redundancy in all nominal operating states, with 2 rotors that have collective and cyclic pitch control, aerosurfaces on the horizontal and vertical stabilizers, and a pusher propeller with minimally collective feathering pitch control (some models include monocyclic for moment generation). This set of controls can be represented by

$$\vec{u} = [\theta_0 \;\; \theta_{lon} \; \theta_{lat} \; \Delta\theta_0 \;\; \Delta\theta_{lon} \; \Delta\theta_{lat} \; \delta_e \; \delta_r \; T_{prop}] \qquad (9)$$

With more controls than are required, some type of allocation scheme is necessary to make best use of all available effectors.

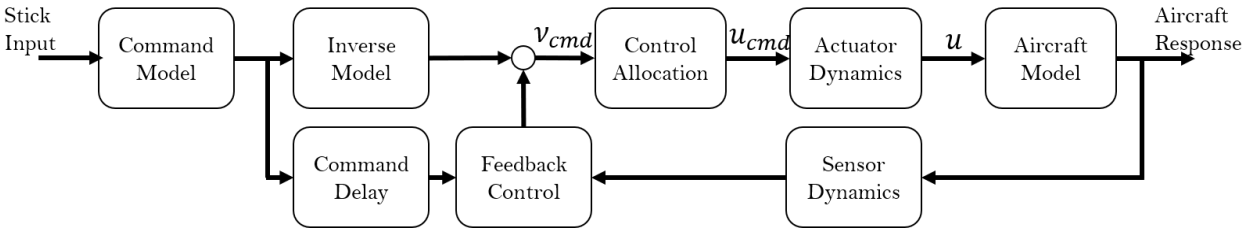

Figure 10. EMF Block Diagram

Table 3. Response Type Summary

Axis	Hover	180 kts
Lateral	RCAH	RCAH
Longitudinal	RCAH	n_z Command/α Hold
Directional	RC DH	β Command/TC
Vertical	RCHH	Direct Stick to Head

Table 4. CONDUIT Specifications

Specification	Axis
Stability Requirements	
Eigenvalue Stability	All
Stability Margins	All
Nichols Margins	All
Handling Qualities Requirements	
Eigenvalue Damping	All
Model Following Cost	All
Bandwidth and Time Delay	R/P/Y
Heave Response	H
Disturbance Rejection Bandwidth/Peak	All
Open Loop Onset Point	All
Minimum Crossover	All
Performance Requirements	
Crossover Frequency	All
Actuator RMS	All

The present study utilizes a weighted pseudoivnerse control allocation, which solves the optimization problem posed as

$$\min ||Wu||_2 \quad s.t. \quad \nu_{cmd} = Bu, \tag{10}$$

$$W_{ii} = \frac{1}{(u_{max} - u_{min})}, \tag{11}$$

where W is a diagonal weighting matrix defined by the position limits of the available controls (Eq. 11) and ν_{cmd} is a vector of desired accelerations. The solution to this problem takes the form

$$u_{cmd} = M\nu_{cmd}, \quad \text{where} \quad M = W^{-1}B^T(BW^{-1}B)^{-1}. \tag{12}$$

Note that only the relevant rows of the B matrix are taken in this formulation, which are the rows for the angular acceleration ($\dot{p}$, $\dot{q}$, $\dot{r}$) equations of the vehicle dynamic response, but could include the vertical acceleration as well if desired. The weighting can be manipulated as desired by the control designer, but typically these weights are defined based on the allowable range of the actuator throw, rate limitations, or some other parameter that reflects the limitation of the actuators relative to one another. In the present study, the allocation for lateral, longitudinal, and directional mixer input are given in Fig. 11.

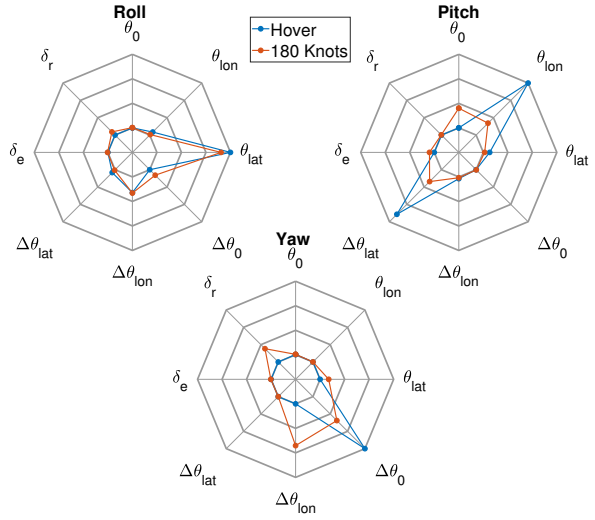

Figure 11. Control Allocation for Hover and Cruise

Summarizing the spider plots given in Fig. 11, the roll control mixer appears similar in hover and in cruise, with some small variation in the relative mixing between θ_{lat} and $\Delta\theta_{lon}$ representing slight changes in the effective control phase angle for the swashplate in this axis. This is expected since there is no aerosurface redundant control in the roll axis. Pitch moment allocation primarily utilizes θ_{lon} and $\Delta\theta_{lat}$ in hover, as is expected because the rotor is the only effective control in this speed. Again, the sharing between symmetric longitudinal and differential lateral cyclic creates additional effective control phasing in the swashplate, with the variation in this sharing more pronounced in the longitudinal axis. At cruise speeds, the pitch moment allocation utilizes the symmetric collective and elevator deflection as well, due to the increased effectiveness of these inputs at higher advance ratio. Finally, the yaw moment allocation utilizes only differential collective in hover, but utilizes a shared control effort between rudder, differential longitudinal, symmetric lateral, and differential collective control. Note that additional weighting could be utilized to favor different controls in hover and in cruise (in order to bias effort away from the rotor if desired), but the results presented here simply utilize the pseudoinverse solution weighted by the position limitations of the effectors.

Control Reconfiguration

In the event of actuator failure in any of the available controls, the control laws (command models, inverse models, feedback gains) themselves are not reconfigured, but the control allocation is redefined such that the failed effector is no longer in use. The method is performed assuming fault detection and identification has occurred. To remove the damaged effector from the allocation, the corresponding column in the B matrix used in Eq. 12 is set to zero and the mixer (M) is recomputed. By solving the problem in this manner, the constraint that $v_{cmd} = Bu$ is enforced and the newly computed control modes still accomplish the same acceleration commanded by the feedback and feedforward control.

SIMULATION RESULTS

A selection of linear simulations are performed in hover and cruise at 180 knots. These cases include piloted maneuvers in a healthy aircraft state, as well as fault cases during steady level flight. In both cases, the aircraft performance will be highlighted and discussed in terms of its tracking performance as well as additional considerations including rotor tip clearance and any undesirable vehicle responses, particularly in fault cases.

Hover Baseline Responses

In hover, the vehicle response to piloted input is chosen as rate command for all axes (RCAH for lateral pitch/roll, RCDH for yaw, and RCHH for vertical). Note that as stated in Ref. 10, this is sufficient to provide Level 1 handling qualities in a Good Visual Environment. A series of piloted maneuvers are presented in Figs. 12-18 to demonstrate the baseline response characteristics of the closed loop system and to highlight trends in the tip clearance behavior of the vehicle.

Figures 12 and 13 depict the aircraft roll response and tip clearance for a simulated pilot lateral cyclic pulse of 25 degrees/second roll rate. Note that the roll rate response is nominally a first order response and the roll attitude follows a step response with some steady state error (approximately 4°), as expected since the vehicle begins to translate. When the maneuver is initiated at 1 second, the rotor tip clearance decreases, then begins to return to the nominal value. Note that the tip clearance does begin to steadily decrease after the stick input ends, which is a result of the vehicle accelerating laterally due to the steady roll attitude and may not be an accurate representation of the vehicle response due to the linear plant dynamics.

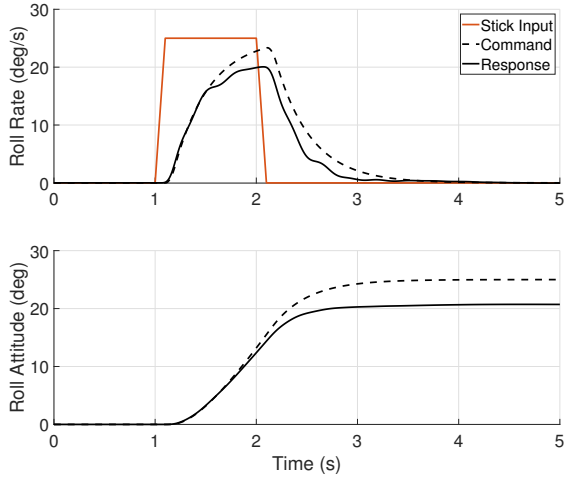

Figure 12. Lateral Cyclic Pulse Roll Response

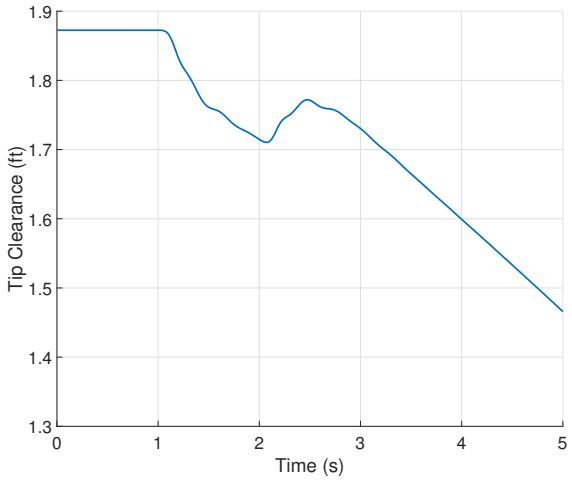

Figure 13. Lateral Cyclic Pulse Tip Clearance Response

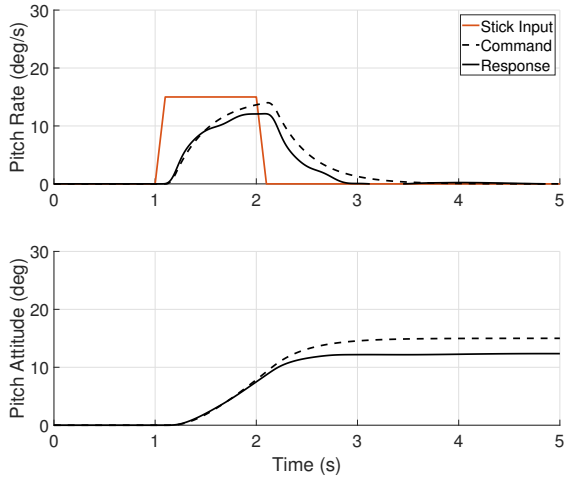

Figure 14. Longitudinal Cyclic Pulse Pitch Response

Similarly, the pitch response and tip clearance are given for a longitudinal cyclic pulse in Figs. 14 and 15. Again, the vehicle follows a first order command from the pulse input and settles with a steady state error in the pitch attitude of 2.7°. The time history of the presented states are similar to the lateral cyclic maneuver, with the primary difference being the magnitude of the rate commanded (15 degrees/second). Again, tip clearance drops at the start of the pilot input and begins to increase again before entering a steady decline as the vehicle accelerates longitudinally away from the hover condition.

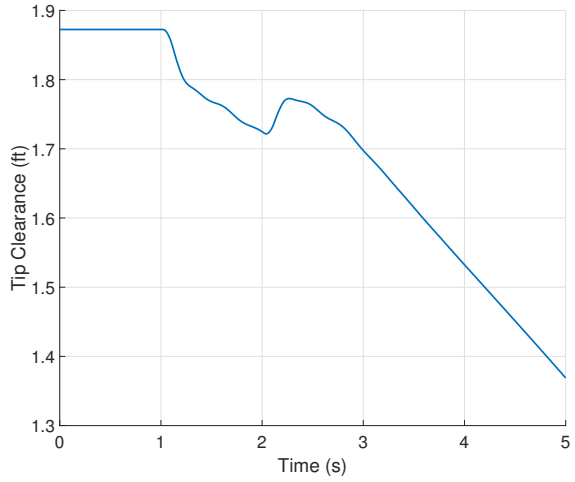

Figure 15. Longitudinal Cyclic Pulse Tip Clearance Response

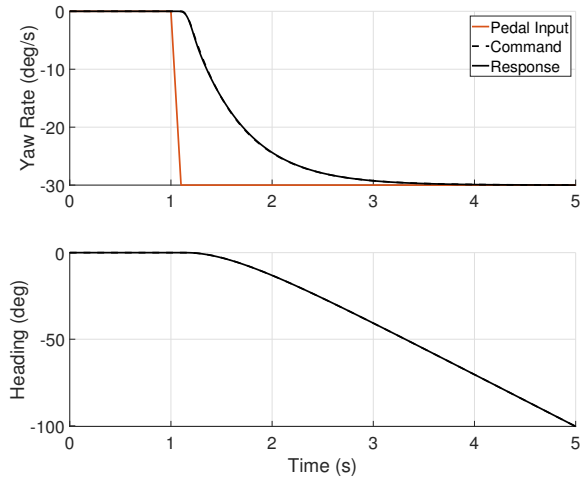

Figure 16. Pedal Kick Yaw Response

Next, a piloted pedal kick is simulated to demonstrate the baseline system performance in yaw. This rate command response is first order, commanding 30 degrees per second of yaw rate (Fig. 16). The system displays excellent command tracking and virtually zero steady state error. Generating the torque required to perform such a maneuver requires differential collective input to the rotor, which results in a differential

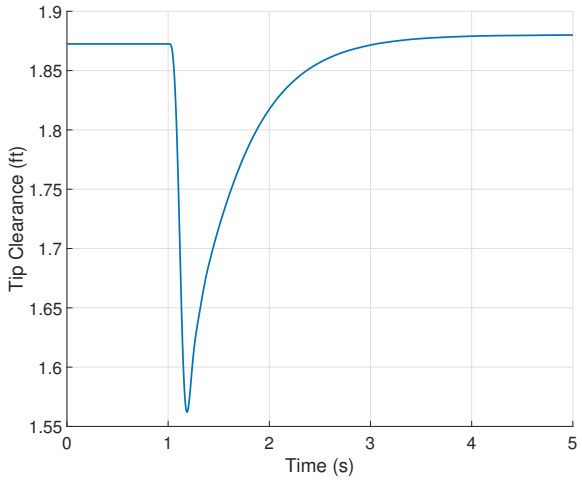

Figure 17. Pedal Kick Tip Clearance Response

coning flap response and a significant change in the tip clearance behavior (Fig. 17).

Lastly, a collective step is simulated for the system, with a pilot commanded climb rate of 1500 feet per second. As was the case in the pedal kick, the system exhibits excellent command tracking of the first order response (Fig. 18). Unlike the pedal kick, however, the thrust required to achieve climb is accomplished with change in symmetric collective pitch, which has little to no effect on the rotor tip clearance, and so is not shown here.

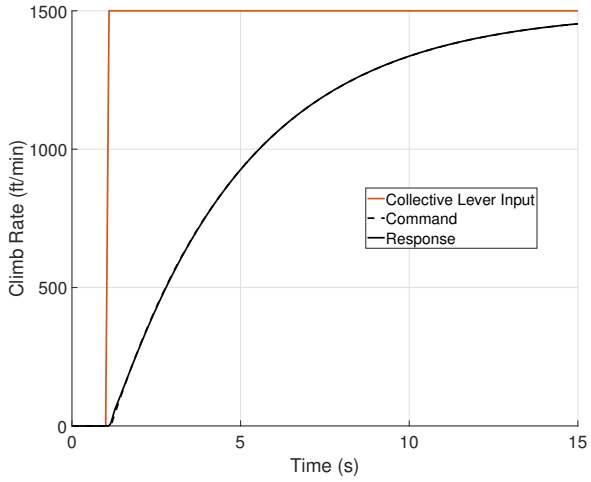

Figure 18. Collective Pull Climb Response

Hover Failure Cases

A selection of swashplate actuator locked failures are considered during steady hover in simulation. In all cases, the actuator being considered is locked 15% above the nominal trim position at 5 seconds. At the same time, the allocator is redefined as described in the approach section in order to best use the available control set. This change in the mixer definition

happens instantly at the time of failure. Because of the symmetry in the hover condition, only two cases are shown here: locked failure of the upper rotor aft and lateral actuators.

The aft swashplate actuator is located at $\psi = -\Gamma = -37.5^\circ$ in the rotor azimuth. Given this location and the stiffness of the coaxial rotor system, it is expected that displacement of this actuator (Fig. 19) from trim will result in a large nose down moment coming from the upper rotor as well as an increase in the rotor thrust resulting from the increase in θ_{1c} and θ_0 on the upper rotor. Note that the commanded position of the upper rotor aft actuator (dashed blue line in the top subfigure of Fig. 19) does not remain flat as was suggested in previous discussion. This is simply because only the roll, pitch, and yaw controls are defined by the pseudoinverse allocator, where the collective control is always defined as symmetric collective pitch applied to both rotors, even after failure. Because in hover the rate command, height hold loop is closed, the collective channel is still active and can result in commands being sent to this failed actuator. As depicted by the sold blue line response, however, the failed actuator does not move once the fault has occurred.

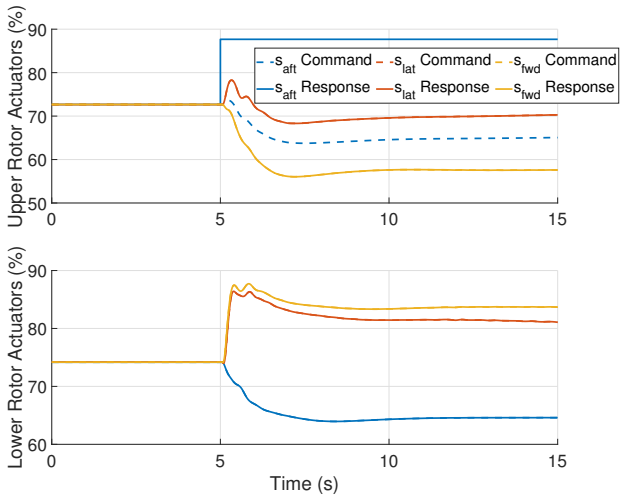

Figure 19. Upper Rotor Aft Actuator Failure Actuator Positions

Failure of the aft actuator results in substantial vehicle motion in the longitudinal axis. Figures 20-23 present the aircraft state trajectory as a result of the failure, including the on and off-axis responses. First, the roll response, given in Fig. 20 is negligible compared to the pitch response in Fig. 21, as would be expected. The disturbance in the pitch response, however, is substantial resulting from the large pitching moment generated by the upper rotor. The deviation in pitch attitude is around 10 degrees at maximum, which places the response in Level 2 according to Table III of ADS-33E (Ref. 24), or acceptable for failures that occur less than 2.5 $\times 10^{-3}$ times per flight hour (once per 400 flight hours).

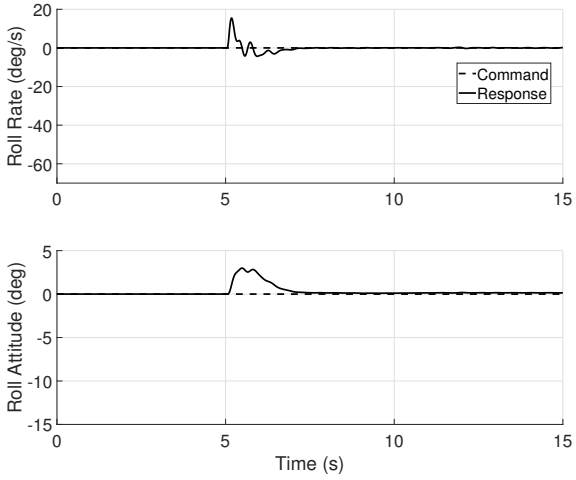

Figure 20. Upper Rotor Aft Actuator Failure Roll Response

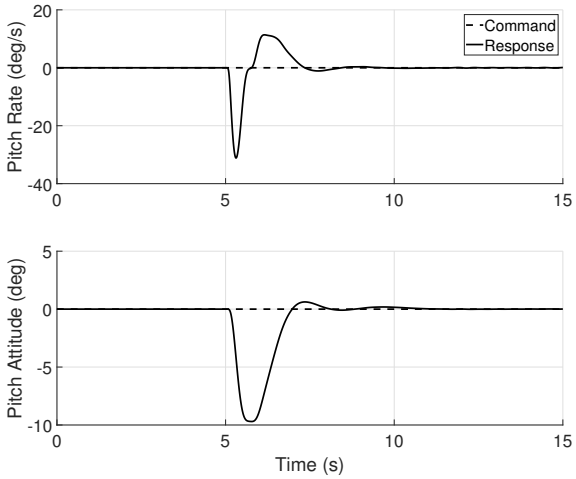

Figure 21. Upper Rotor Aft Actuator Failure Pitch Response

The failure of the aft actuator changes the mean collective pitch of the upper rotor, which generates a change in the rotor thrust and torque. This results in the vehicle entering a climb and yawing motion when failure occurs (Figs. 22 and 23).

Following from the actuator position time history given in Fig. 19, the resulting rotor head controls are given in Fig. 24. Primary compensation is achieved by a reduction of the lateral and forward actuators on the upper swashplate to reduce the collective pitch, while mirroring the actuator positions on the lower rotor. This mirrored response results in a substantial differential longitudinal cyclic input (green curve in Fig. 24), which leads to a significant differential longitudinal flap response and a reduction in the rotor tip clearance (Fig. 25). Note that this tip clearance violates the flight test observed tip clearance for the X2TD of 11 inches ($\sim$ 0.92 feet) defined in Ref. 22 "to ensure margin during initial envelope expansion."

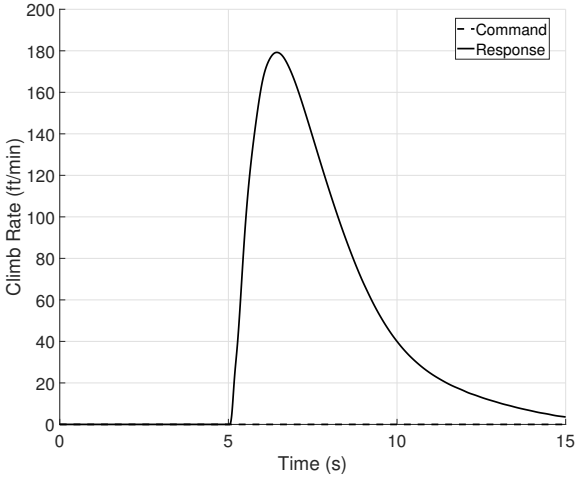

Figure 22. Upper Rotor Aft Actuator Failure Climb Rate

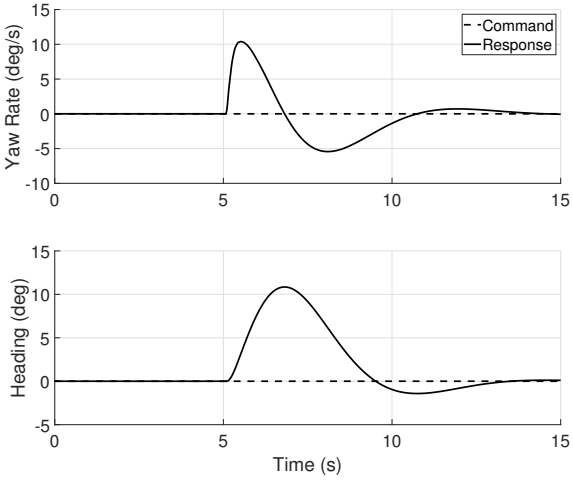

Figure 23. Upper Rotor Aft Actuator Failure Yaw Response

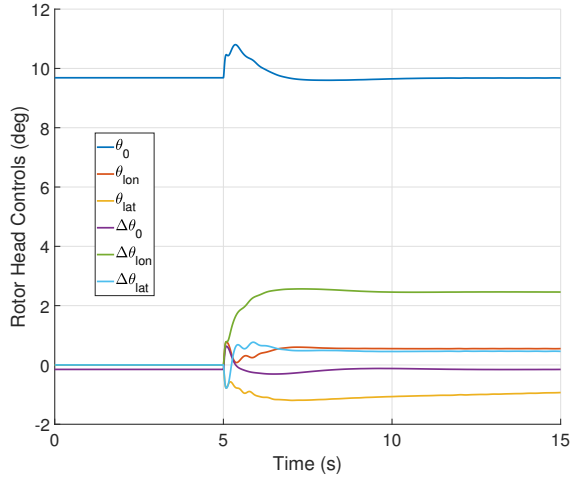

Figure 24. Upper Rotor Aft Actuator Failure Rotor Head Controls

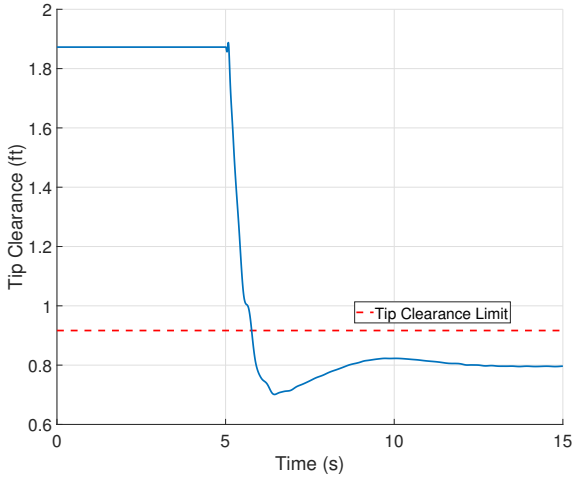

Figure 25. Upper Rotor Aft Actuator Failure Tip Clearance

The lateral actuator failure case is similar to the aft actuator case, except the primary vehicle response is in roll , because the lateral actuator on the upper rotor swashplate is located at $\psi = 90^\circ - \Gamma = 52.5^\circ$ on the counter-clockwise azimuth, so locking above the trim position generates positive lateral cyclic and a negative (roll-left) rolling moment from the upper rotor. Actuator fault is considered in the same manner as the aft actuator case, and actuator position time histories are given in Fig. 26. Note again that the lateral actuator does receive commands from the collective channel input, but does not respond after 5 seconds.

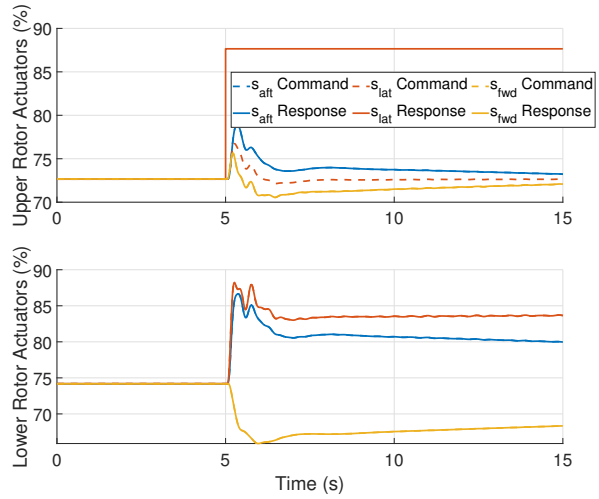

Figure 26. Upper Rotor Lateral Actuator Failure Actuator Positions

Similar to the aft actuator failure case, the resultant hub moment of the upper rotor results in significant vehicle motion. However, because this fault case perturbs the lateral cyclic of the upper rotor primarily, the dominant motion is in roll, shown in Fig. 27. Compared to the aft actuator failure case, this roll response is significantly larger, and the transient roll

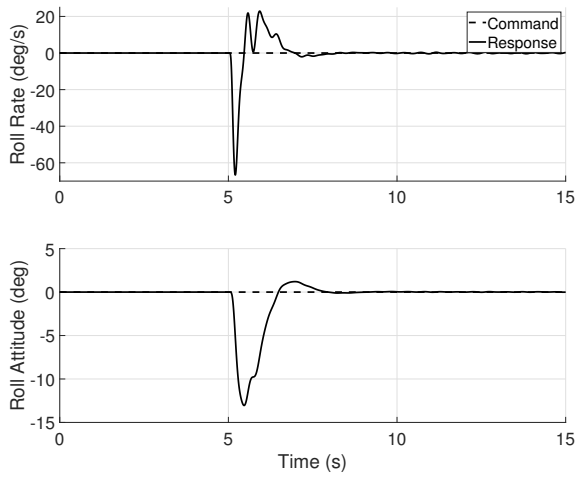

Figure 27. Upper Rotor Lateral Actuator Failure Roll Response

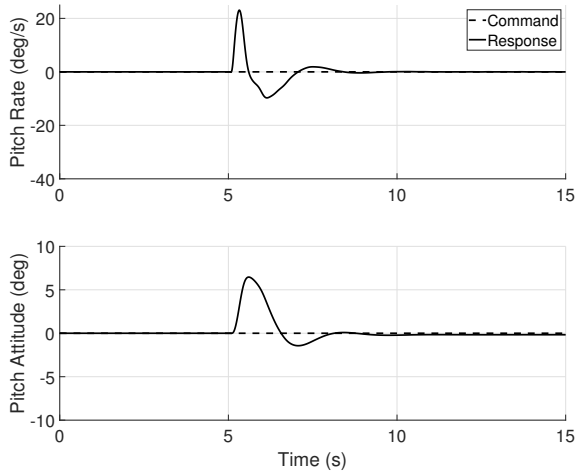

Figure 28. Upper Rotor Lateral Actuator Failure pitch Response

attitude response falls to Level 3 according to Table III in ADS-33E (Ref. 24), which is acceptable for failures that occur less than 2.5×10^{-5} times per flight hour (once per 40,000 flight hours). For completeness, the pitch response to the upper rotor lateral actuator failure is included in Fig. 28. This response is small compared to the roll response, in the same way that the roll response was significantly smaller than the pitch response for the aft actuator fault case. This indicates that the position of the actuators largely contribute to on-axis responses, shifting the position of these actuators would result in different amounts of inter-axis coupling.

The movement of the lateral swashplate actuator does increase the mean collective pitch, but because of the swashplate geometry, this influence is roughly half of what the aft actuator caused for the same displacement from trim. As a result, the climb rate (Fig. 29) and yaw response (Fig. 30) are smaller than the aft actuator case, and the change in the collective setting can be seen in Fig. 31 to compare with the aft failure case.

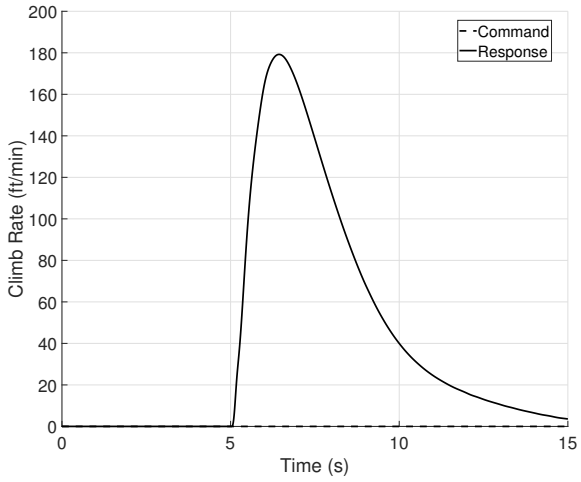

Figure 29. Upper Rotor Lateral Actuator Failure Climb Rate

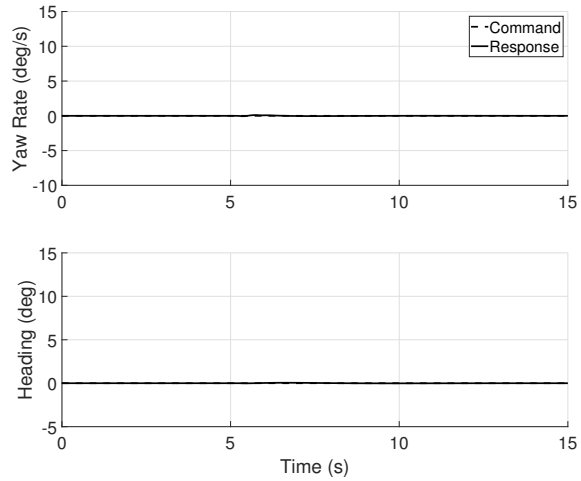

Figure 30. Upper Rotor Lateral Actuator Failure Yaw Response

Finally, the compensation for the lateral actuator failure (Fig. 26) requires a similar set of rotor head controls (Fig. 31) relative to the aft actuator fault case, but utilization of differential lateral cyclic (light blue line in Fig. 31) instead of differential longitudinal. However, the rotor tip clearance (Fig 32) is still reduced in a similar manner through differential lateral flapping, which follows from the similar amount of differential cyclic used in comparison to the aft actuator fault case. Again, this failure case violates the observed tip clearance limit for the X2TD.

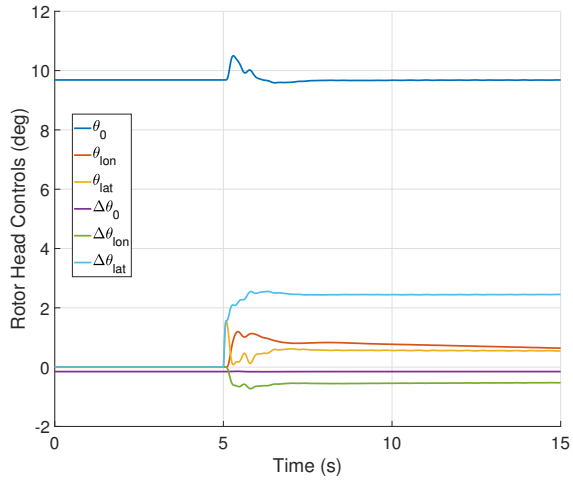

Figure 31. Upper Rotor Lateral Actuator Failure Rotor Head Controls

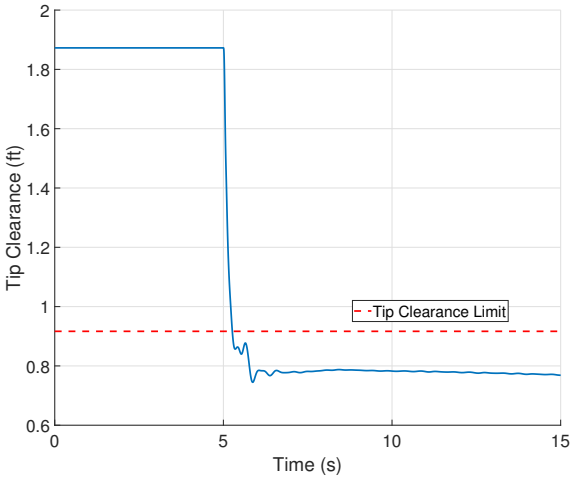

Figure 32. Upper Rotor Lateral Actuator Failure Tip Clearance

180 Knot Baseline Response

At 180 knots the response to pilot input is changed in every control axis except lateral cyclic, which remains RCAH. The longitudinal cyclic now controls stability axis vertical acceleration (n_z) command, angle of attack hold, pedal input controls sideslip command, turn coordination, and the collective lever is now direct stick-to-head control, where the symmetric collective pitch of the rotor system is directly commanded by the collective lever position. The longitudinal stick response changes from rate command to stability axis vertical acceleration (n_z) command in order to stabilize the short period mode present in the plant dynamics. This approach was also taken on the generic coaxial-pusher simulation model developed by the Army (Ref. 10). The pedal response change to sideslip command in cruise allows for automatic turn coordination and is typical for high-speed vehicles. As was done for the hover condition, the baseline stick responses are presented here for reference.

The lateral stick response is very similar to that presented in Fig. 12, with the exception that the commanded rate is larger representing the larger maximum attainable roll rate requirement of 90 degrees/second for Level 1 piloted handling qualities in forward flight (the present study provides 50% maximum rate commands for reference). The roll rate and attitude are given in Fig. 33, and the corresponding tip clearance is given in Fig. 34. Note that because of the zero sideslip angle commanded by zero pedal deflection, the vehicle also enters a coordinated turn, indicated by the nonzero steady yaw rate in Fig. 35. The larger transient behavior in the tip clearance response can be attributed to the additional control effort required to maintain the coordinated turn.

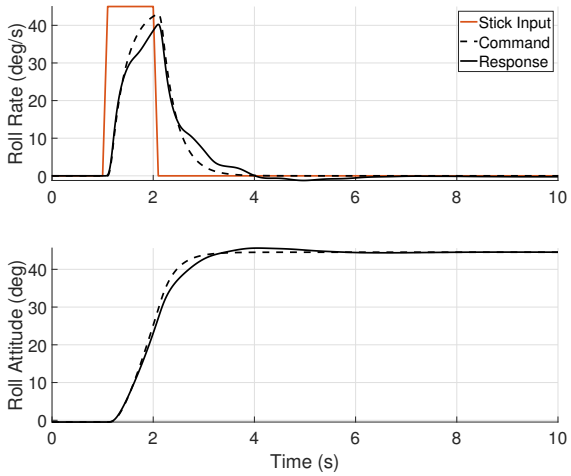

Figure 33. Lateral Cyclic Pulse Roll Response, Cruise

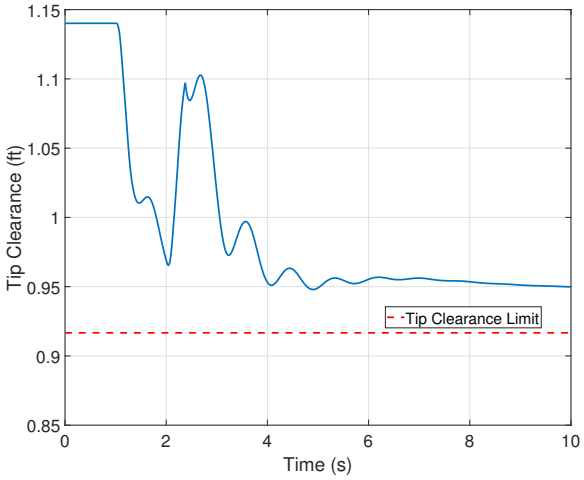

Figure 34. Lateral Cyclic Pulse Tip Clearance, Cruise

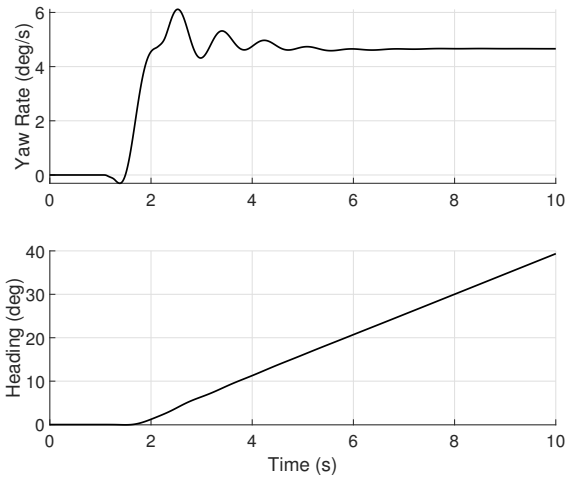

Figure 35. Lateral Cyclic Pulse Yaw Response, Cruise

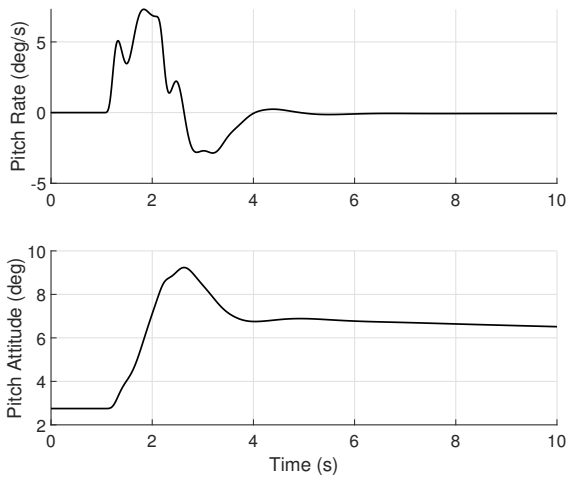

Figure 37. Longitudinal Cyclic Pulse Pitch Response, Cruise

A baseline longitudinal response to a 0.75 g pulse command is given in Fig. 36. Stability axis vertical acceleration is achieved with a pitching motion of the vehicle, as indicated by the pitch response given in Fig. 37.

Note that this response doesn't follow the same type of trajectory as a typical pitch rate response, but does pitch the aircraft nose up an additional 3° after the piloted input has ended. This results in a substantial climb rate, given in Fig. 38. The tip clearance for the maneuver is shown in Fig. 39. Note that the primary use of the rotor controls in the pitch allocation results in a large tip clearance response that violates the 11 inch (0.92 feet) clearance limit, which suggests that more careful design of the weights in the allocation should be considered to utilize the elevator more heavily.

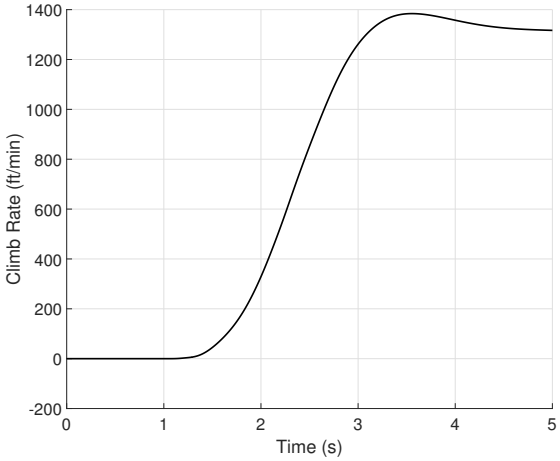

Figure 38. Longitudinal Cyclic Pulse Climb Rate, Cruise

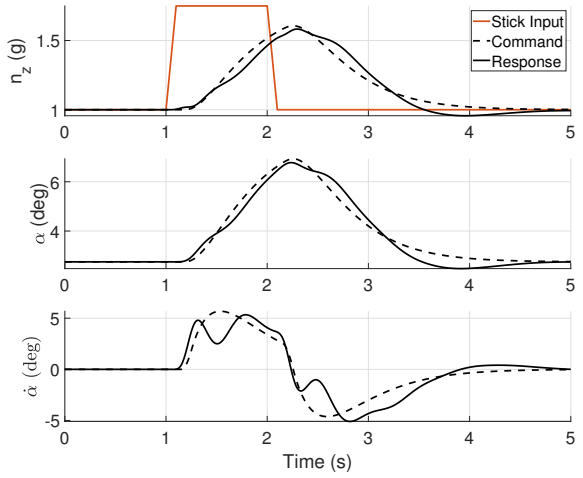

Figure 36. Longitudinal Cyclic Pulse n_z and α Response, Cruise

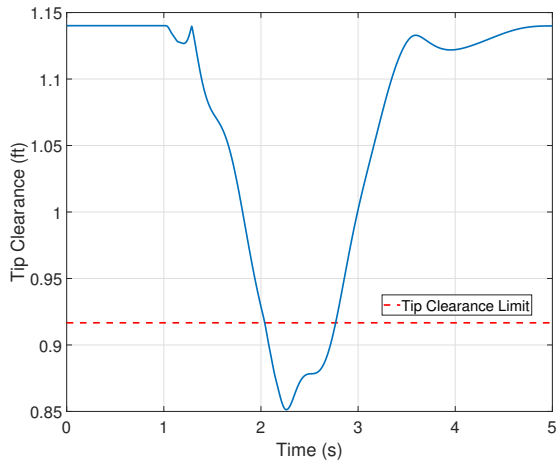

Figure 39. Longitudinal Cyclic Pulse Tip Clearance, Cruise

The response to pedal input is given in Fig. 40, with tip clearance given in Fig. 41. Note that the baseline control allocation utilizes differential rotor inputs along with the rudder to accomplish the desired sideslip response, resulting in a large reduction in the rotor tip clearance and eventual intersection of the rotor planes (negative tip clearance values). However, as indicated in Fig. 41, changing the relative authority of the rudder versus the rotor controls (by applying a different weighting scheme in the pseudoinverse optimization) can yield different tip clearance trends while accomplishing the same commanded response by utilizing more rudder control and less rotor controls. The corresponding rotor controls (yawing torque is accomplished primarily by the presented controls) and rudder input are provided in Figs. 42 and 43. This highlights the need for more careful design of the control allocation, especially for yaw control, rather than a simple application of the pseudoinverse. It should also be noted that use of the rotor system to generate a yawing moment has a dramatic impact on rotor tip clearance, which will make failure in the rudder a difficult problem, to be discussed later.

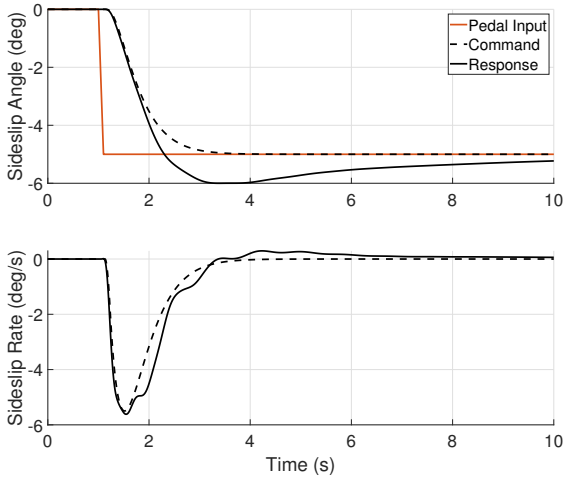

Figure 40. Pedal Kick Sideslip Response, Cruise

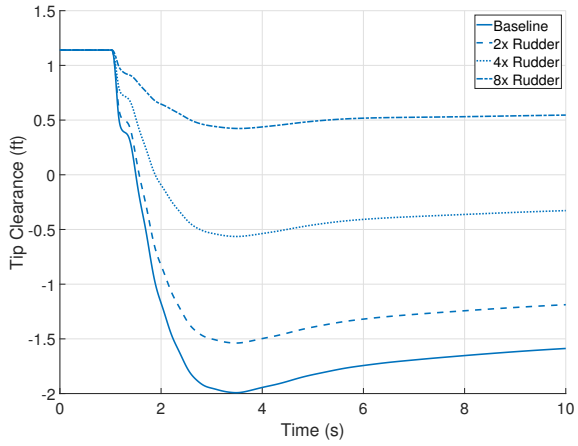

Figure 41. Pedal Kick Tip Clearance, Cruise

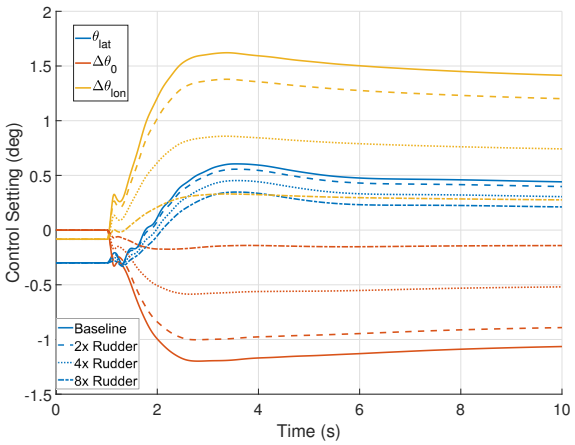

Figure 42. Pedal Kick Rotor Head Controls, Cruise

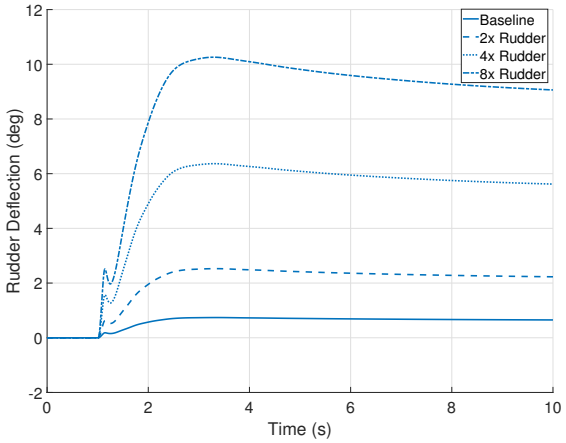

Figure 43. Pedal Kick Rudder Input, Cruise

180 Knot Failure Cases

Strictly speaking, all available actuators have a possibility of fault in all vehicle operating states. However, the present study considers only failure of the aerosurfaces (elevator and rudder) in the cruise condition. This approach is taken for brevity and also due to the fact that swashplate actuator failure appears at least notionally similar in hover and in cruise, with the difference being that undesired rotor hub force and moment can now be at least partially compensated for by the empennage surfaces instead of necessarily requiring differential moments in the rotor system.

Elevator fault is simulated by moving the surface from trim at -5° (trailing edge up) back to zero deflection at 5 seconds (Fig. 44). This new setting introduces a transient response, where the vehicle experiences a nose-down pitching moment and consequently a negative pitch rate and new trim pitch attitude at approximately nose-level (Fig. 45).

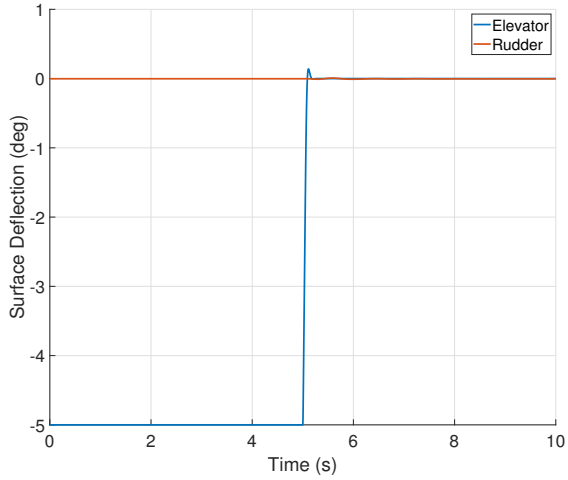

Figure 44. Elevator Failure Aerosurface Time History, Cruise

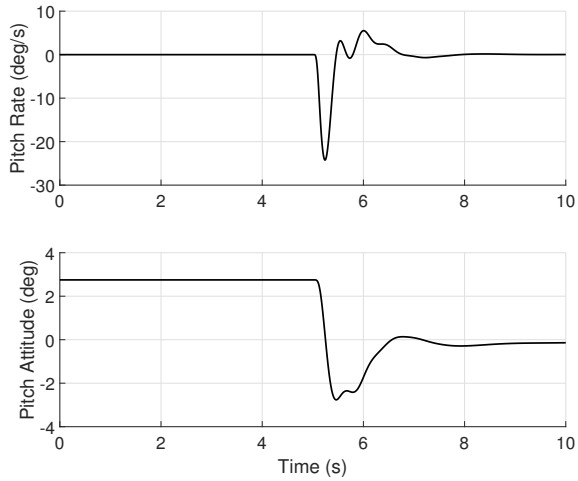

Figure 45. Elevator Failure Pitch Response, Cruise

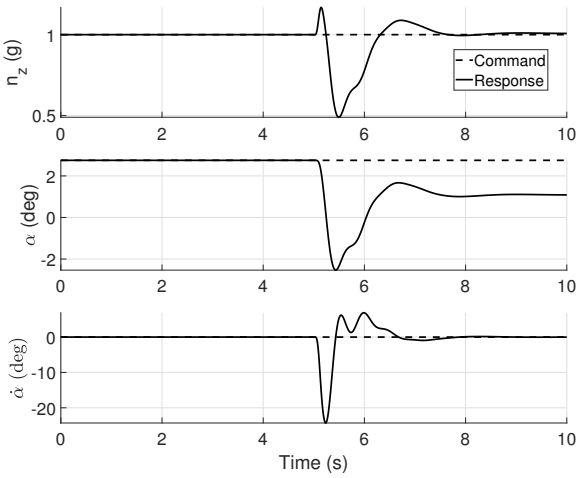

Figure 46. Elevator Failure n_z and α Response, Cruise

Because the longitudinal command is now n_z, the aircraft now returns to the nominal trim state of $n_z = 1g$ (Fig. 46), with a change in the vehicle angle of attack corresponding to the new steady pitch attitude.

Compensation for elevator failure requires the balancing of vehicle pitching moment and vertical force in order to drive n_z back to its nominal value of 1g. Without a functional elevator, the rotor controls are the only viable options as the rudder produces no significant longitudinal or vertical forcing. The time history of the rotor controls, given in Fig. 47, show that the rotor pitch controls that are primarily shown in Fig. 11 are utilized at the time of failure, combining to restore trim. Note that using these rotor controls to compensate for the sudden disturbance caused by the elevator failure changes the flapping state of the rotor system, resulting in a significant tip clearance transient (Fig. 48).

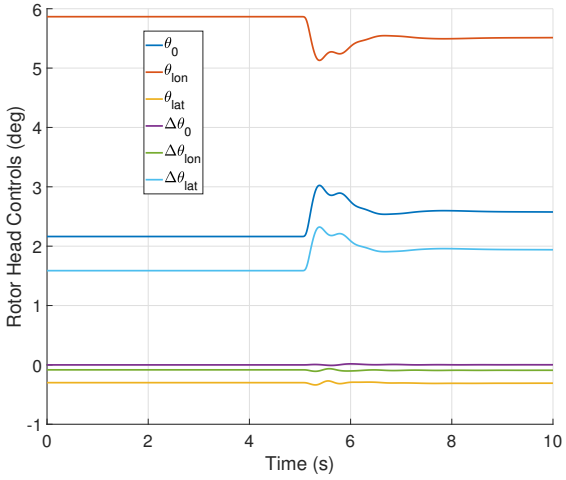

Figure 47. Elevator Failure Rotor Head Controls, Cruise

The behavior exhibited in the tip clearance again indicates that different weights should be considered in the weighted pseudoinverse to prevent large tip clearance deviation, perhaps including the lateral and longitudinal differential flapping dynamics in the optimization problem. Note that a forward path control as was implemented for the generic coax (Ref. 10) would not improve this response, as the response here is all from the feedback system (zero pilot commands).

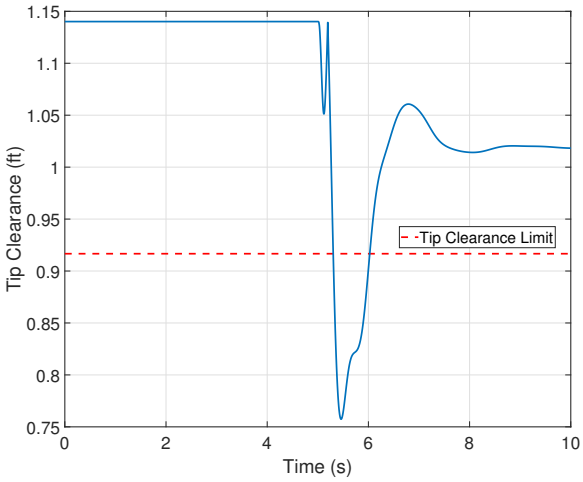

Figure 48. Elevator Failure Tip Clearance, Cruise

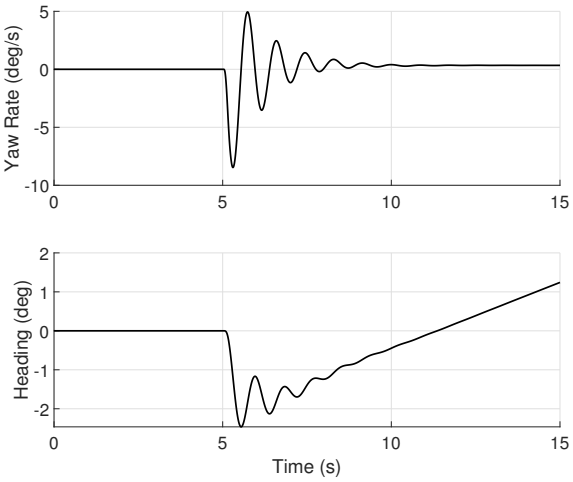

Figure 50. Rudder Failure Yaw Response, Cruise

Rudder failure in a coaxial helicopter system is particularly challenging, due to the lack of efficient yawing moment generation from the dual rotor system in cruise. Granted, the rotor has enough control power to generate any required moment for reasonable yaw rate or sideslip commands, but this requires use of differential inputs to the rotor system. Differential inputs in general force the rotor into differential flapping states, which leads to reduction in tip clearance or even blade strike when large enough directional input is commanded. To illustrate this problem, the rudder is moved out of trim (at $\delta_r = 0°$) to a -5 degree position at 5 seconds simulation time (Fig. 49).

This new setting generates a nose-right yawing moment (Fig. 50), which requires the rotor to compensate using differential controls (Fig. 51).

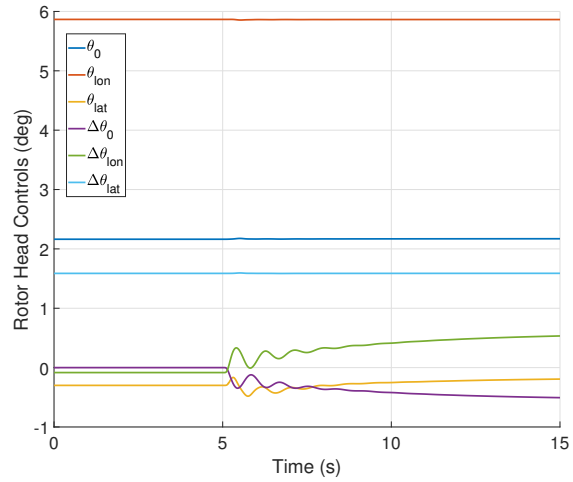

Figure 51. Rudder Failure Rotor Head Controls, Cruise

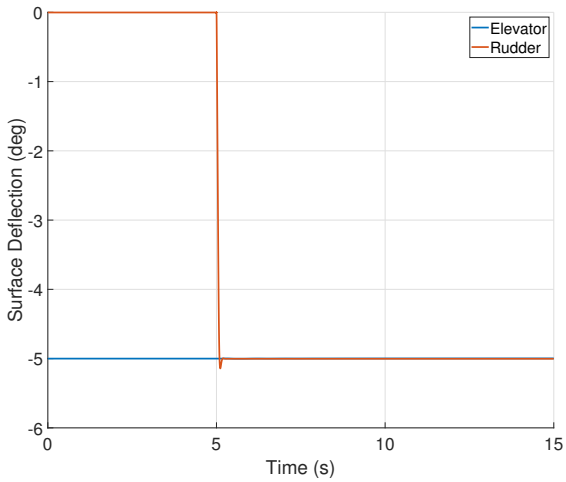

Figure 49. Rudder Failure Aerosurface Time History, Cruise

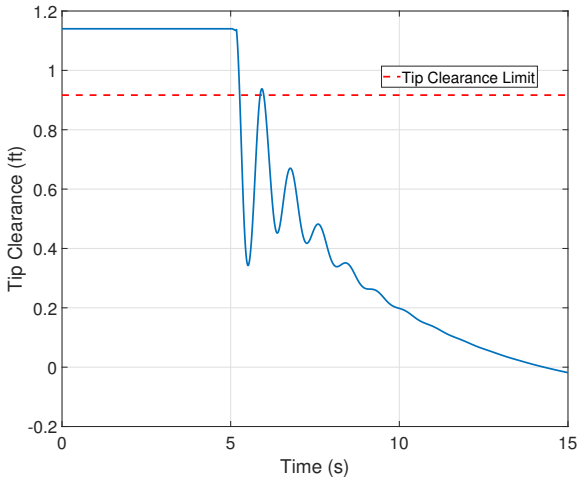

Figure 52. Rudder Failure Tip Clearance, Cruise

As shown in Fig. 42, the primary controls that can be used to generate this net rotor hub torque are $\Delta\theta_0$, $\Delta\theta_{lon}$ and θ_{lat}, which are primarily differential moment generators, and so the rotor tip clearance is significantly impacted by this fault case (Fig. 52), eventually leading to a tip strike. Note that the total rudder range of deflection is $\pm 30^\circ$, so this locked position of 5° represents a fairly small deflection. Larger displacements of the rudder would in turn require larger compensation, at further detriment to the rotor tip clearance. This further illustrates the need for careful consideration of directional control authority on a coaxial helicopter platform; the addition of effectors such as propeller monocyclic (or other effectors that don't directly influence rotor flap behavior) may be required to ensure sufficient resilience to rudder failure. Even post-failure, once the vehicle has returned to trim, the ability of the aircraft to perform a yawing maneuver without violating any observed tip clearance limits will be greatly impacted. If no additional effector is available outside of the rotor controls, it may be necessary to limit the directional input that the pilot can command in order to maintain safe flight, at the cost of handling qualities performance.

CONCLUSIONS

This paper described and presented validation of the RPI Coaxial Helicopter Analysis and Dynamics code (CHAD), with results based on the Sikorsky X2 Technology™ Demonstrator. Validation was provided both in steady trim results as well as bare airframe frequency responses, both cases were compared to measured and identified published flight test data. An explicit model following control system was designed using CONDUIT® for both hover and cruise at 180 knots using a weighted pseudoinverse control allocation. Different baseline flight conditions and failure cases were examined to investigate the performance of the vehicle with flight control failure in flight. The following conclusions are drawn:

1. The coaxial model (CHAD) showed good agreement with published flight test data both in steady trim and bare airframe frequency responses. Key dynamic modes were well predicted, including the hovering cubic peak and lead-lag dipole in the hover condition.

2. Weighted pseudoinverse control allocation generated optimal control modes to distribute demanded moments among the available actuators in nominal conditions. This approach allowed for recalculation of the allocation in failure modes, resulting in a stable control system post failure.

3. Yaw control needs to be designed carefully so as to make use of controls that do not directly impact the tip clearance of the vehicle. Results presented show that the nominal pseudoinverse yaw allocation results in a negative tip clearance, but additional weighting can bias control effort to the rudder to limit the reduction in tip clearance.

4. The recalculated peeudoinverse approach performed well in terms of the vehicle recovering steady state after a failure has occurred. In every fault case considered in this study, the aircraft returns to trim within 5 seconds of the failure with no additional pilot intervention required.

5. In hover, the aircraft can tolerate locked failures of the swashplate actuators. However, this requires substantial differential cyclic input, resulting in a differential flap response. As was demonstrated, this reduces the rotor tip clearance substantially, which effectively reduces the range in which an actuator can fail and still maintain a safe operating condition.

6. In cruise, elevator failure is easily compensated with a combination of symmetric collective pitch and symmetric longitudinal along with differential lateral cyclic (to change the effective control phase angle). This redistribution of the pitch moment results in fairly large tip clearance reduction during the transient, but this effect can likely be mitigated with refined control weighting in the pseudoinverse. Failure of the rudder is more challenging because of the differential controls required, resulting in large reductions in rotor tip clearance. Additional effectors may be required for yaw control to allow for resilience to rudder failure.

AUTHOR CONTACT:

Michael McKay	mckay2@rpi.edu
Praneet Vayalali	vayalp@rpi.edu
Farhan Gandhi	fgandhi@rpi.edu

ACKNOWLEDGMENTS

This work is carried out at the Rensselaer Polytechnic Institute under the Army/Navy/NASA Vertical Lift Research Center of Excellence (VLRCOE) Program, grant number W911W61120012, with Dr. Mahendra Bhagwat as a Technical Monitor. The authors would also like to acknowledge the Department of Defense and the Army Research Office for sponsoring Mr. McKay through the National Defense Science and Engineering Graduate Fellowship.

REFERENCES

1. F. Colucci, "The Moving Parts of Future Vertical Lift," *Vertiflite*, pp. 12–16, Oct. 2019.

2. G. Jacobellis, F. Gandhi, and M. Floros, "Using Control Redundancy for Power and Vibration Reduction on a Coaxial Rotor Helicopter at High Speeds," *Journal of the American Helicopter Society*, vol. 64, pp. 1–15, July 2019.

3. J. P. Reddinger, F. Gandhi, and H. Kang, "Using Control Redundancy for Power and Vibration Reduction on a Compound Helicopter at High Speeds," *Journal of the American Helicopter Society*, vol. 63, pp. 1–13, July 2018.

4. J. P. Reddinger and F. Gandhi, "Physics-Based Trim Optimization of an Articulated Slowed-Rotor Compound Helicopter in High-Speed Flight," *Journal of Aircraft*, vol. 52, pp. 1756–1766, Dec. 2015.

5. T. Herrmann, R. Celi, and J. Baeder, "Multidisciplinary Trim Analysis of a Coaxial-Pusher Rotorcraft Configuration," in *American Helicopter Society 74th Annual Forum, Phoenix, AZ*, May 2018.

6. T. Herrmann, R. Celi, and J. Baeder, "Multidisciplinary, Multiobjective Trim Optimization for a Coaxial-Pusher Rotorcraft Configuration," in *Vertical Flight Society 75th Annual Forum, Philadelphia, PA*, May 2019.

7. T. Berger, O. Juhasz, M. J. S. Lopez, M. B. Tischler, and J. F. Horn, "Modeling and Control of Lift Offset Coaxial and Tiltrotor Rotorcraft," *CEAS Aeronautical Journal*, 2019.

8. C. Fegely, O. Juhasz, H. Xin, and M. B. Tischler, "Flight Dynamics and Control Modeling with System Identification Validation of the Sikorsky X2 Technology Demonstrator," in *American Helicopter Society 72nd Annual Forum, West Palm Beach, FL*, May 2016.

9. O. Juhasz, H. Xin, and M. B. Tischler, "Inflow Based Flight Dynamics Modeling Improvements for the Sikorsky X2 Technology™Demonstrator," in *American Helicopter Society 76th Annual Forum (Virtual)*, Oct. 2020.

10. T. Berger, C. L. Blanken, M. B. Tischler, and J. F. Horn, "Flight Control Design and Simulation Handling Qualities Assessment of High-Speed Rotorcraft," in *Vertical Flight Society 75th Annual Forum, Philadelphia, PA*, May 2019.

11. T. Berger, M. B. Tischler, and J. F. Horn, "Outer-Loop Control Design and Simulation Handling Qualities Assessment for a Coaxial-Compound Helicopter and Tiltrotor," in *Vertical Flight Society 76th Annual Forum, Virtual*, Oct. 2020.

12. J. P. Reddinger and F. Gandhi, "Using Redundant Effectors to Trim a Compound Helicopter with Damaged Main Rotor Controls," in *American Helicopter Society 73rd Annual Forum, Fort Worth, TX*, May 2017.

13. P. Vayalali, M. McKay, and F. Gandhi, "Redistributed Pseudoinverse Control Allocation for Actuator Failure on a Compound Helicopter," in *American Helicopter Society 76th Annual Forum (Virtual)*, Oct. 2020.

14. P. Vayalali, M. Mckay, J. Krishnamurthi, and F. Gandhi, "Horizontal Stabilator Utilization for Post Swashplate Failure Operation on a UH-60 Black Hawk Helicopter," *Journal of the American Helicopter Society*, vol. 65, pp. 1–13(13), Apr. 2020.

15. P. Vayalali, M. McKay, J. Krishnamurthi, and F. Gandhi, "Fault-Tolerant Control on a UH-60 Black Hawk helicopter using horizontal stabilator," *CEAS Aeronautical Journal*, Oct 2020.

16. M. E. Knapp, C. M. Ivler, J. F. Horn, E. N. Johnson, D. O. Bridges, M. J. Lopez, M. B. Tischler, J. A. Wagster, and K. K. Cheung, "Development and Simulation of Damage Tolerant Control Laws for a Compound Helicopter," in *AIAA SciTech 2020 Forum, Orlando, FL*, Jan. 2020.

17. M. McKay, P. Vayalali, and F. Gandhi, "Post-Failure Control Reconfiguration on a High-Speed Lift-Offset Coaxial Helicopter," in *American Helicopter Society 76th Annual Forum (Virtual)*, Oct. 2020.

18. Y. B. Kong, J. V. R. Prasad, and D. Peters, "Development of a Finite State Dynamic Inflow Model for Coaxial Rotor using Analytical Methods," in *American Helicopter Society 73rd Annual Forum, Fort Worth, TX*, May 2017.

19. R. D. Harrington, "Full-Scale-Tunnel Investigation of the Static-Thrust Performance of a Coaxial Helicopter Rotor," techreport 2318, National Advisory Commitee For Aeronautics (NACA), Mar. 1951.

20. R. Feil, J. Rauleder, C. Cameron, and J. Sirohi, "Aeromechanics Analysis of a High Advance Ratio Lift Offset Coaxial Rotor System," *Journal of Aircraft*, vol. 56, pp. 166–178, Jan. 2019.

21. S. W. Ferguson, "A Mathematical Model for Real Time Flight Simulation of a Generic Tilt-Rotor Aircraft," CR 166536, NASA, Sept. 1988.

22. D. Walsh, S. Weiner, K. Arifian, T. Lawrence, M. Wilson, T. Millott, and R. Blackwell, "High Airspeed Testing of the Sikorsky X2 Technology Demonstrator," in *American Helicopter Society 67th Annual Forum, Virginina Beach, VA*, May 2011.

23. M. Tischler, T. Berger, C. Ivler, M. Mansur, K. Cheung, and J. Soong, *Practical Methods for Aircraft and Rotorcraft Flight Control Design: An Optimization-Based Approach*. Reston, VA: AIAA Education Series, 2017.

24. Anon, "Handling Qualities Requirements for Military Rotorcraft," tech. rep., Aeronautical Design Standard and Performance, Specification ADS-33E-PRF, US Army Aviation and Missile Command, 2000.